Insect Biochemistry and Molecular Biology 148 (2022) 103813

Contents lists available at ScienceDirect

Insect Biochemistry and Molecular Biology

journal homepage: www.elsevier.com/locate/ibmb

Sequential phase I metabolism of pyrethroids by duplicated CYP6P9 variants results in the loss of the terminal benzene moiety and determines resistance in the malaria mosquito *Anopheles funestus*

Melanie Nolden [a,b], Mark J.I. Paine [b,**], Ralf Nauen [a,*]

[a] Bayer AG, Crop Science Division, Alfred Nobel Str. 50, D-40789, Monheim am Rhein, Germany
[b] Department of Vector Biology, Liverpool School of Tropical Medicine, Pembroke Place, Liverpool, L3 5QA, United Kingdom

ARTICLE INFO

Keywords:
Cytochrome P450
Vector control
Pyrethroid
Insecticide
Resistance
Anopheles

ABSTRACT

Pyrethroid resistance in *Anopheles funestus* is threatening the eradication of malaria. One of the major drivers of pyrethroid resistance in *An. funestus* are cytochrome P450 monooxygenases CYP6P9a and CYP6P9b, which are found upregulated in resistant *An. funestus* populations from Sub-Saharan Africa and are known to metabolise pyrethroids. Here, we have functionally expressed CYP6P9a and CYP6P9b variants and investigated their interactions with azole-fungicides and pyrethroids. Some azole fungicides such as prochloraz inhibited CYP6P9a and CYP6P9b at nanomolar concentrations, whereas pyrethroids were weak inhibitors (>100 μM). Amino acid sequence comparisons suggested that a valine to isoleucine substitution at position 310 in the active site cavity of CYP6P9a and CYP6P9b, respectively, might affect substrate binding and metabolism. We therefore swapped the residues by site directed mutagenesis to produce CYP6P9a^{I310V} and CYP6P9b^{V310I}. CYP6P9b^{V310I} produced stronger metabolic activity towards coumarin substrates and pyrethroids, particularly permethrin. The V310I mutation was previously also detected in a pyrethroid resistant field population of *An. funestus* in Benin. Additionally, we found the first metabolite of permethrin and deltamethrin after hydroxylation, 4′OH permethrin and 4′OH deltamethrin, were also suitable substrates for CYP6P9-variants, and were depleted by both enzymes to a higher extent than as their respective parent compounds (approximately 20% more active). Further, we found that both metabolites were toxic against *An. funestus* FANG (pyrethroid susceptible) but not towards FUMOZ-R (pyrethroid resistant) mosquitoes, the latter suggesting detoxification by overexpressed CYP6P9a and CYP6P9b. We confirmed by mass-spectrometric analysis that CYP6P9a and CYP6P9b are capable of cleaving phenoxybenzyl-ethers in type I pyrethroid permethrin and type II pyrethroid deltamethrin and that both enzymes preferentially metabolise trans-permethrin. This provides new insight into the metabolism of pyrethroids and a greater understanding of the molecular mechanisms of pyrethroid resistance in *An. funestus*.

1. Introduction

In 2020 Malaria caused 627 000 deaths globally, with the large majority (602 000 deaths) occurring in Africa (WHO, 2021). The use of interventions such as insecticide treated bednets (ITN) and indoor residual sprays (IRS) to control indoor biting mosquitoes was estimated to have been responsible for ~80% of the reduction in Malaria cases from 2000 to 2019 (Bhatt et al., 2015; WHO, 2020). Until recently pyrethroids were the only insecticidal class used in ITN thus driving the rapid spread of pyrethroid resistance in *Anopheles* populations across the African continent (WHO, 2018). Pyrethroid resistance is mainly conferred by an altered target, the voltage gated sodium channel (VGSC), and/or upregulated P450 enzymes, which are responsible for phase I xenobiotic metabolism and clearance (David et al., 2013; Martinez-Torres et al., 1998; Nauen et al., 2022; Ranson et al., 2011).

Pyrethroids are synthetic insecticides derived from the natural compound pyrethrin. They are designated as type I and type II pyrethroids based on the respective absence or presence of an *alpha*-cyano group, which enhances the toxicity of the insecticide (Soderlund, 2020). Permethrin and deltamethrin, type I and II pyrethroids respectively, are amongst the most widely used insecticides for vector control applications. Structurally similar, they share a phenoxybenzyl moiety and a

* Corresponding author.
** Corresponding author.
E-mail addresses: Mark.Paine@lstmed.ac.uk (M.J.I. Paine), ralf.nauen@bayer.com (R. Nauen).

https://doi.org/10.1016/j.ibmb.2022.103813
Received 8 June 2022; Received in revised form 17 July 2022; Accepted 17 July 2022
Available online 21 July 2022

cyclopropane ring. It is widely accepted that the 4'para position of the phenoxybenzyl structure is the preferred site of oxidation by insect P450s (Ruzo et al., 1978; Stevenson et al., 2011; Nolden et al., 2022; Zimmer et al., 2014), along with other routes of metabolism including hydroxylation of the gem-dimethyl site or ester-cleavage (Casida et al., 1983; Shono et al., 1979). Furthermore, analysis of deltamethrin metabolism by *Anopheles gambiae* CYP6M2 has revealed that sequential breakdown of the 4′-hydroxy deltamethrin primary metabolite can occur (Stevenson et al., 2011) as well as ether-cleavage of the diphenyl moiety., To date CYP6M2 is the only insect P450 enzyme in which this has been shown (Feyereisen, 2019). Permethrin is composed of four different isomers (R-cis, S-cis, R-trans and S-trans) although their individual interactions with P450 enzymes are not clear. Structurally different pyrethroids, such as etofenprox (non-ester-pyrethroid), bifenthrin or transfluthrin are also used as insecticides, where fluorination of P450 sites of oxidation can limit metabolism and reduce cross-resistance (Moyes et al., 2021; Zimmer and Nauen, 2011).

Anopheles funestus s.s. is a major vector for the transmission of malaria in Africa. Unlike *An. gambiae* and many other Anopheline malaria vectors, knock down resistance (*kdr*) mutations to the voltage gated sodium channel are uncommon (Irving and Wondji, 2017). Instead, pyrethroid resistance is driven primarily by metabolic mechanisms that are predominantly associated with the upregulation of P450 enzymes (Amenya et al., 2008; Ibrahim et al., 2016, 2018; Riveron et al., 2013, 2014). These include CYP6P9a and CYP6P9b, which are the result of a gene duplication event and often highly expressed in pyrethroid resistant field populations of *An. funestus* as well as the laboratory reference strain FUMOZ-R (Nolden et al., 2021; Wondji et al., 2022). Since inhibition of P450 activity can revert metabolic resistant mosquitoes to a susceptible phenotype (Brooke et al., 2001), the inclusion of piperonyl butoxide (PBO), a strong P450 inhibitor, is being used in the latest generation of pyrethroid treated bednets to combat pyrethroid resistance (Gleave et al., 2018; Protopopoff et al., 2018). We have recently shown that BOMFC is a highly active fluorescent probe substrate for recombinant CYP6P9a and CYP6P9b (Nolden et al., 2022), and demonstrated that azole fungicides are also efficient inhibitors of P450 activity in microsomal preparations of *An. funestus,* recommending further characterization of their interactions with individual P450s associated with pyrethroid resistance (Nolden et al., 2021).

CYP6P9a and CYP6P9b can metabolise pyrethroids (Riveron et al., 2013, 2014; Yunta et al., 2019), although detailed biochemical characterisation of their interactions with pyrethroid substrates and products of metabolism are lacking. The two P450s are highly similar sharing 94% amino acid sequence identity (Fig. S1a). While this suggests a similar substrate profile, even single amino acid changes can have a profound effect on substrate binding, altering substrate specificity and metabolism (Paine et al., 2003). We were therefore interested in comparing the interactions of CYP6P9a and CYP6P9b with pyrethroid insecticides and azole inhibitors and to identify amino acid residues in the active sites of the enzymes that might differentiate substrate binding and metabolism. As a starting point we focussed on I-helix amino acid residue 310, which is close (~10 Å) to the reactive heme iron centre and different between CYP6P9a and CYP6P9b. It is present as an isoleucine residue in CYP6P9a and valine in CYP6P9b (Fig. S1b).

In this study, we have compared the enzymatic activity of the recombinantly expressed gene duplicates, *CYP6P9a* and *CYP6P9b* against various substrates. We have also used mass-spectrometry to identify the products of deltamethrin, racemic permethrin (and its *cis*- and *trans*-diastereomers) metabolism by CYP6P9a and CYP6P9b and the mechanism of substrate breakdown. We have carried out site-directed mutagenesis to create two mutants CYP6P9a^{I310V} and CYP6P9b^{V310I} to compare their metabolic activity with CYP6P9a and CYP6P9b towards permethrin, deltamethrin and fluorescent probe substrates to examine the role of amino acid 310 in CYP6P9a/b substrate metabolism. Our results provide a new understanding of the metabolic fate of common type I and type II pyrethroids in the malaria mosquito *An. funestus* that will aid in the development of new resistance-breaking compounds used in vector control applications.

2. Materials and methods

2.1. Mosquitoes

An. funestus FANG and FUMOZ-R mosquitoes were reared as recently described by Nolden et al. (2021). In brief: both strains were kept at 27.5 °C ± 0.5 °C, 65% ± 5% relative humidity and a photoperiod of 12/12 L:D with 1h dusk/dawn. Adults were kept in rearing cages (46 cm × 33 cm x 20 cm) and five days after hatching the first blood meal (bovine blood, obtained from Elocin Laboratory, Oberhausen, Germany) was provided according to standard protocols (Das et al., 2007).

2.2. Chemicals

Deltamethrin (CAS: 52918-63-5), permethrin (CAS: 52645-53-1; 61.3% trans- and 30.5% cis permethrin), β-nicotinamide adenine dinucleotide 2′-phosphate (NADPH) reduced tetrasodium salt hydrate (CAS: 2646-71-1 anhydrous, purity ≥93%), 7-ethoxycoumarin (EC; CAS: 31005-02-4, >99%), 7-methoxy-4-trifluoromethylcoumarin (MFC; CAS: 575-04-2, ≥99%), 7-Ethoxy-4-trifluoromethylcoumarin (EFC; CAS: 115453-82-2, ≥98%) 7-benzyloxy-4-trifluoromethylcoumarin (BFC; CAS: 220001-53-6, ≥99%), 7- hydroxy-coumarin (HC; CAS: 93-35-6, 99%) 7-hydroxy-4-trifluoromethylcoumarin (HFC; CAS: 575-03-1, 98) were purchased from Sigma Aldrich/Merck (Darmstadt, Germany). Cis-permethrin (CAS: 61949-76-6) and trans-permethrin (CAS: 61949-77-7) were purchased from Dr. Ehrenstorfer (LGC group, Teddington, UK). 7-benzyloxymethoxy-4-trifluoromethylcoumarin (BOMFC; CAS: 277309-33-8; purity 95%) was synthesized by Enamine (Riga, Latvia). 4′OH permethrin (CAS: 67328-58-9 ≥ 97%) was synthetized by Aragen (formerly GVK Bio, Hyderabad, India). 7-pentoxycoumarin and 4′OH-deltamethrin (CAS: 66855-89-8) were internally synthetized (Bayer AG, Leverkusen, Germany). All chemicals were of analytical grade unless otherwise stated.

2.3. Glazed tile bioassay

To generate dose-response curves of 4′OH-deltamethrin, 4′OH permethrin and cis- and trans-permethrin, *An. funestus* FANG and FUMOZ-R mosquitoes were exposed to a range of different concentrations in a glazed tile assay as recently described by Nolden et al. (2021). Insecticides were dissolved in acetone with a starting concentration of 100 mg/m^2 and diluted in 1:5 steps to 0.0064 mg/m^2. Using an Eppendorf pipette 1.125 μl of each concentration was applied onto a glazed tile (15 cm × 15 cm, ceramic, Vitra, Germany). After the evaporation of acetone and mosquito recovery from anaesthetation (1 h), female adults were exposed in triplicate (n = 10) for 30 min to each insecticide concentration and afterwards transferred back to an untreated paper card and kept in Petri dishes overnight. A 10% dextrose solution was provided overnight as a food source. Mortality was scored 24 h post-exposure. Acetone alone served as a control. Control mortality between 5 and 20% was corrected using Abbott's formula (Abbott, 1925), and bioassays exceeding 20% control mortality were considered invalid.

2.4. Heterologous expression of CYP6P9a and CYP6P9b

Heterologous baculovirus expression was conducted as previously described by (Nolden et al., 2022). In brief: sequence information of CYP6P9a/b from *An. funestus* and NADPH cytochrome P450 reductase (CPR) from *An. gambiae* (AgCPR) were obtained from GenBank (Table S1) and plasmids were created using GeneArt server (ThermoFisher). As a vector pFastBac1 and as restrictions sites BamHI and HindIII were chosen. Plasmids were transformed into MaxEfficiancyDH10

(Invitrogen, 10361012) competent cells according to manufacturer's instructions. The virus was transfected into Sf9 cells (Gibco, kept in Sf-900-SFM (1X) cell culture medium, containing 25 μg/mL gentamycin) and titre was determined employing Rapid Titer Kit (Clontech, 631406).

High five cells were kept in Express five medium (SFM (1X), Gibco, 10486–025) containing 18 mM Glutamax (100X, Gibco, 35050–061) and 10 μg/mL gentamycin (Gibco, 1670–037). Cells were incubated with 0.5% fetal bovine serum (FBS; Sigma Aldrich, F2442), 0.2 mM delta-aminolevulinic acid (d-ALA; CAS: 5451-09-2, Sigma Aldrich), 0.2 mM Fe III citrate (CAS: 2338-05-8, Sigma Aldrich) and the respective amount of virus. After harvesting, cells were resuspended in buffer (0.1 M K_2HPO4, 1 mM DTT, 1 mM EDTA, 200 mM saccharose, pH 7.6). FastPrep device (MP Biomedicals, Irvine, CA, USA) was used for shredding the cells followed by a 10-min centrifugation step at 4 °C and 700×*g* (Eppendorf). The supernatant was centrifuged for 1 h at 100 000×*g* and 4 °C (Beckman, rotor: 45TI). The resulting microsomal pellet was resuspended in buffer (0.1 M K_2HPO4, 0.1 mM EDTA, 1 mM DTT, 5% Glycerol, pH 7.6) and protein amount was determined.

Carbon monoxide (CO)-difference spectra were generated according to (Omura and Sato, 1964) in order to calculate K_{cat} values. Mock cells served as controls throughout the study as well as microsomal fractions without NADPH regeneration system.

2.5. Computational analysis, modelling and docking experiments

CYP6P9a (AFUN015792-RA) and CYP6P9b (AFUN015889-RA) transcripts show 92.7% nucleotide identity and translated protein sequences are 94.3% identical (Geneious alignment, Geneious 10.2.6; Fig. S1a). Substrate recognition sites (SRS) were assigned to CYP6P9a and CYP6P9b based on CYP2A1 (*Rattus norvegicus*, GenBank NP_036824.1) according to Gotoh (1992). To predict and analyse the potential metabolism of probe substrates and pyrethroids, 3D-homology models of CYP6P9a and CYP6P9b based on the crystal structure of human CYP3A4 (PDB: 1TQN) were created. 3D-structures of BOMFC, deltamethrin and permethrin were received from PubChem (https://pubchem.ncbi.nlm.nih.gov/) and transformed into PDB files using Chimera (USCF Chimera, Version 1.15). After performing dock-prep in Chimera, AutoDock Vina (Version 1.1.2) using Chimera software was performed, with a 20 $Å^3$ squared volume around the heme (Oleg and Olson, 2010). Five docking scenarios for each substrate were generated and analysed based on score (binding affinity kcal/mol) and putative sites of metabolic attack.

2.6. Site-directed mutagenesis of amino acid residue 310

In CYP6P9a isoleucine 310 is translated by the codon ATC at position 927–929 (transcript), in CYP6P9b valine is translated by GTG at position 927–929. We created two mutants: CYP6P9a I310V ($CYP6P9a^{I310V}$) and CYP6P9b V310I ($CYP6P9b^{V310I}$). Generated pFastBac vectors (as described above) containing either CYP6P9a or CYP6P9b were used for site-directed mutagenesis using a Q5-site-directed mutagenesis Kit following manufacturer's instructions (New England Biolabs, E0554). Specific primers were generated using NEBaseChanger (https://nebasechanger.neb.com/) (Table S1). Twenty-five ng of total plasmid DNA and each primer with a final concentration of 0.5 μM in 25 μl reactions were used. PCR conditions were as follows: 98 °C for 30 s, followed by 25 cycles of 98 °C for 10 s, 66 °C for 30 s and 72 °C for 3 min and 10 s. Final extension step was at 72 °C for 2 min. A kinase, ligase and DpnI (KLD) treatment containing 1 μl PCR Product, 5 μl KLD Reaction buffer, 10X KLD Enzyme Mix and 3 μl Nuclease-free water was added and incubated at room temperature for 5 min. Afterwards 5 μl of KLD mix was added to 5-alpha-competent *E. coli* cells for transformation (New England Biolabs, C2987H) following manufacturer's instructions. Cells were diluted 10- and 40-times and incubated overnight on LB-Agar plates (MP biomedicals, 113002201-CF, capsules, concentration: 40 g/L) containing carbenicillin (100 μg/ml, CAS: 4800-94-6). Mini- (3 ml) and Midi (25 ml) preps in LB medium (MP biomedicals, 113002011-CF, capsules, concentration: 25 g/L) containing 100 μg/ml carbenicillin were generated and plasmids were isolated using Qiafilter Plasmid Midi Kit following manufacturer's instructions (Qiagen, 12243, Hilden, Germany). DNA concentrations were photometrically determined using 260/280 ratio (NanoQuant Infinite 200, Tecan, Switzerland) and normalized to 100 ng/μl. To confirm successful mutagenesis, samples were sent for sequencing (TubeSeq Service, Eurofins). Sequencing primers can be found in Table S1. Plasmids containing substituted nucleotides were further processed as described above.

2.7. P450 activity assays with fluorinated coumarin probe substrates

P450 enzyme assays were conducted as previously described by Haas and Nauen (2021) with minor changes. Substrate competition kinetics were evaluated using eleven different BOMFC, BFC and EFC concentrations (stock 50 mM in DMSO) between 200 μM and 0.195 μM, diluted in 0.1 M potassium-phosphate buffer (pH 7.6) containing 0.01% zwittergent 3–10 (CAS 15163-36-7, Sigma-Aldrich), a range of pyrethroid concentrations (100, 10, 1 μM final concentration (fc)) and 1 mM NADPH at 20 °C ± 1 °C. Enzymes were diluted to 0.16 mg/ml in buffer (0.1 M K_2HPO4, 0.1 mM EDTA, 1 mM DTT, 5% glycerol pH 7.6), 0.05% bovine serum albumin (BSA), 0.01% zwittergent 3–10 – finally corresponding to 4 μg protein per 25 μl enzyme solution. Twenty-five μl enzyme solution and 25 μl substrate solution were incubated for 1 h in a black 384-well plate and the reaction stopped by adding 50 μl of red-ox mix (25% DMSO, 50 mM Tris–HCl buffer (pH 10), 5 mM glutathione oxidized, and 0.2 U glutathione reductase). Each reaction was replicated four times and the fluorescent product HFC was measured at 405 nm while excited at 510 nm. Substrate saturation kinetics were analysed using GraphPad Prism 9.0 and were analysed for competitive, non-competitive, and mixed-type inhibition (assuming Michaelis-Menten kinetics).

2.8. Inhibition assays with CYP6P9 variants

IC_{50} analysis was performed as previously described in Nolden et al. (2021) with minor modifications. Assay conditions were optimized for linearity in time and protein amount. Eleven concentrations of inhibitors and pyrethroids (pre-diluted in DMSO in 1:3.3 steps, final DMSO concentration (1%), except for epoxiconazole (2%)) to a final assay concentration ranging from 100 μM to 0.000596 μM in 0.1 M potassium-phosphate-buffer (pH 7.6). Microsomal fractions were diluted to a final amount of 4 μg of protein per 100 μl in buffer (0.1 M K_2HPO4, 0.1 mM EDTA, 1 mM DTT, 5% glycerol pH 7.6) containing 0.01% zwittergent and 0.05% BSA. Enzymes were incubated with inhibitors and pyrethroids for 10 min at 20 °C ± 1 °C. Afterwards 25 μl 20 μM BOMFC solution (10 μM final concentration, the approximate K_m for all variants) containing 0.125 mM (fc) NADPH was added. Each reaction was replicated four times, stopped after 30 min by adding stopping solution and evaluated as described above. Inhibition was analysed using GraphPad Prism 9.0 four-parameter, non-linear regression model. Reactions containing no inhibitor served as controls.

2.9. UPLC-MS/MS analysis and pyrethroid metabolite quantification

Metabolism assays were conducted as previously described by Nolden et al. (2022) with minor changes. Deltamethrin and permethrin metabolism and quantification of the respective 4′OH-deltamethrin and 4′OH permethrin were assessed using UPLC-MS/MS analysis. Recombinantly expressed CYP6P9 variants and mutants were co-expressed with *An. gambiae* CPR (P450:CPR at MOI 1:0.5) and diluted to 0.8 mg protein ml^{-1} in buffer (0.1 M K2HPO4, 1 mM DTT, 0.1 mM EDTA, 5% Glycerol, pH 7.6). Forty μl of recombinant proteins were incubated in 96-deepwell plates (Protein lobind, Eppendorf) in 100 μl reactions with

10 μM deltamethrin, permethrin or the respective 4′OH metabolite (solved in DMSO and further diluted to 100 μM in 0.1 M K_2HPO_4, 0.05% bovine serum albumin (BSA), pH 7.6) and 50 μl of assay buffer containing NADPH-regeneration system (Promega, V9510). As control, wells without regeneration system and microsomal fractions from a control (mock) virus were included. The reactions were incubated at 450 rpm and 30 °C (Thermomixer, Eppendorf) and stopped with 400 μl ice-cold acetonitrile (100%) after 90 min. Plates were stored at 4 °C overnight, centrifuged (3220×*g*, 4 °C, 30 min, Eppendorf 5810 R) and the resulting supernatant was transferred into a 1000 ml collection plate (186002481, Waters, Eschborn, Germany).

UPLC-MS/MS chromatography was carried out using an Agilent 1290 Infinity II system with a Waters Acquity BEH C18 (50 × 2.1 mm, 1.7 μm) column and eluted with methanol, 2 mM ammonium acetate, and water, 2 mM ammonium acetate with 1% acetic acid in gradient mode. After positive electrospray ionization, ion transitions were recorded on a Sciex API6500 Qtrap. Ion transition was as followed: for deltamethrin 523 > 281, for 4′OH-deltamethrin 539 > 281, for permethrin 183.051 > 152.200 and for 4′OH-permethrin 424.079 > 199.200. In positive ion mode the peak integrals were calibrated externally against a standard calibration curve. Samples were diluted prior to measurement if needed. Linear ranges were as followed: For deltamethrin: 0.5–500 ng/ml, for 4′OH deltamethrin: 0.3–100 ng/ml, for permethrin: 0.1–120 ng/ml (cis) and 0.05–26 ng/ml (trans) and for 4′OH-permethrin: 0.05–23 ng/ml (cis) and 0.1–27 ng/ml (trans). UPLC-TOF-MS was employed using an Acquity UPLC I-Class system coupled to a cyclic iMS mass spectrophotometer (Waters Corporation, MA, USA) as recently described (Haas et al., 2021). The mass spectrometer operated in positive ion mode for deltamethrin and permethrin and in negative ion mode for the respective 4′OH metabolites with a full scan resolution at 60 000 fwhm (full width at half maximum). Measurements and metabolite searches were conducted with MassLynx and MetaboLynx software (Waters Corporation, MA, USA).

3. Results

3.1. Inhibition potential of azole fungicides, pyrethroids and PBO towards CYP6P9a and CYP6P9b

The interactions of CYP6P9a and CYP6P9b with deltamethrin and permethrin and their primary metabolites 4′OH deltamethrin and 4′OH permethrin were compared by measuring their kinetic effects on the inhibition of the *O*-debenzylation of the fluorescent probe substrate BOMFC at three concentrations (100 μM, 10 μM and 1 μM) (Fig. 1 and Table S2). The P450s showed a similar pattern of inhibition producing much weaker inhibition of BOMFC *O*-debenzylation with the parent deltamethrin and permethrin compounds compared with strong inhibition by 4′OH permethrin and 4′OH deltamethrin (Table 1). Inhibition by the 4′OH metabolites also produced an increase in K_m alongside significant decreases in reaction rate (V_{max}), indicating a mixed-type inhibition and no clear competitive inhibition (Table S2). For example, the V_{max} of CYP6P9a BOMFC *O*-debenzylation decreased from 191 pmol product/min x mg protein^{-1} to 104 pmol product/min x mg protein^{-1} in the presence of 100 μM 4′OH deltamethrin, with a concomitant K_m increase from 8.64 μM to 74.8 μM suggesting BOMFC displacement (Table S2).

Several pyrethroids, azole fungicides, and PBO were tested against CYP6P9a and CYP6P9b to evaluate their potential to inhibit *O*-debenzylation of BOMFC (Table 1). Overall, similar patterns of inhibition were observed, with the strongest inhibitor being prochloraz with IC_{50} values

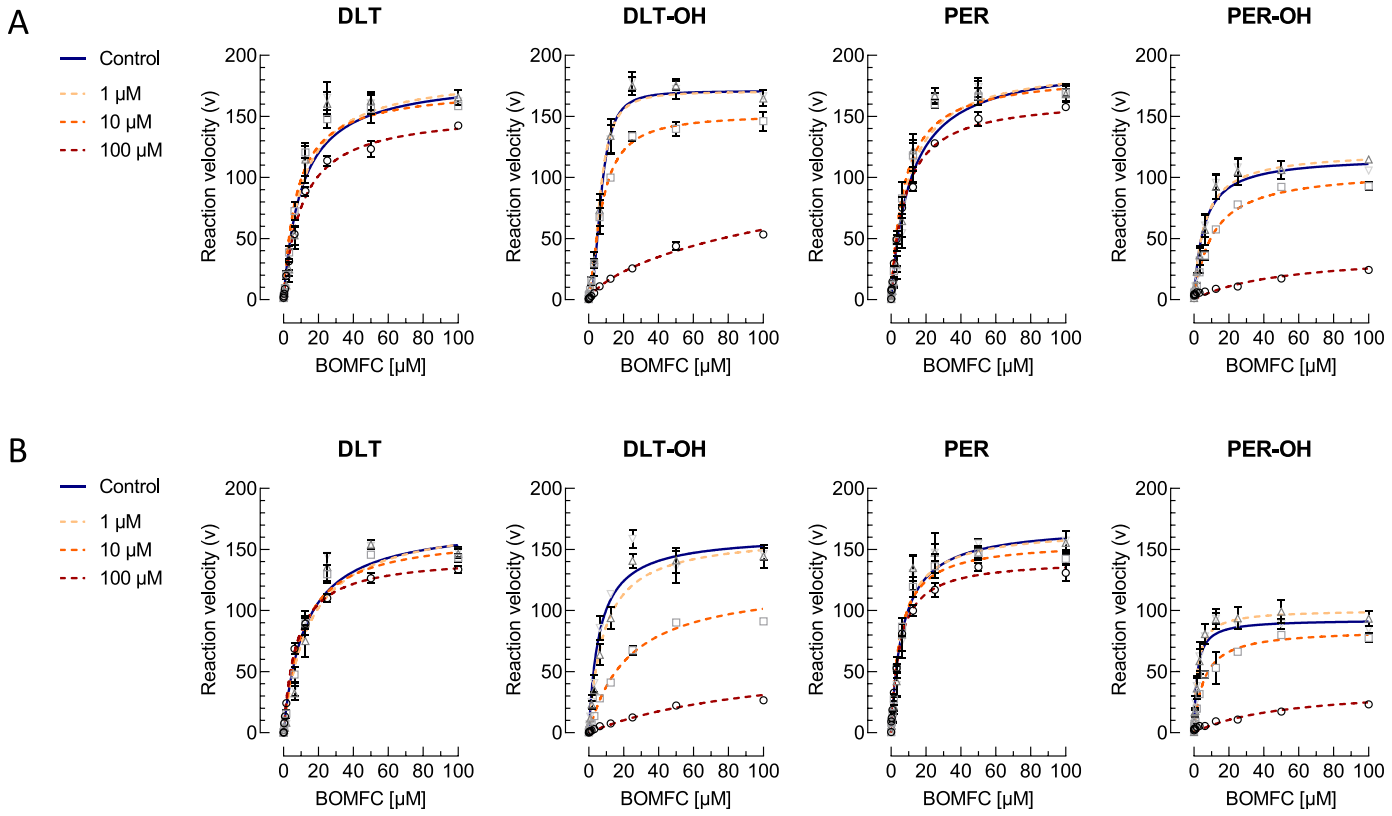

Fig. 1. Effect of different pyrethroid substrates on the O-debenzylation of 7-benzyloxymethoxy-4-(trifluoromethyl)-coumarin (BOMFC) by recombinantly expressed *An. funestus* CYP6P9 variants. Michaelis–Menten kinetics of (A) CYP96P9a- and (B) CYP6P9b-mediated BOMFC metabolism using increasing concentrations of deltamethrin (DLT), 4′OH deltamethrin (DLT-OH), permethrin (PER) and 4′OH permethrin (PER-OH). Data are mean values ± SD (n = 4). Reaction velocity is defined as pmol 7-hydroxy-4-trifluoromethylcoumarin (HFC)/min x mg protein. Details on Michaelis-Menten kinetic data analysis are given in the supporting information (Table S2).

Table 1
Biochemical analysis of CYP6P9 variant interaction with different compounds in fluorescence assays. Inhibition of O-debenzylation of 7-benzyloxymethoxy-4-(trifluoromethyl)-coumarin (BOMFC) by recombinantly expressed *An. funestus* CYP6P9a and CYP6P9b by pyrethroid insecticides, their metabolites and common P450 inhibitors. Date are mean values ± 95% CI (n = 4).

Compound	CYP6P9a		CYP6P9b	
	IC_{50} [μM]	95% CI	IC_{50} [μM]	95% CI
Deltamethrin	>100		>100	
4′OH Deltamethrin	6.28	4.83–8.06	1.75	1.53–1.99
Permethrin	>100		>100	
4′OH Permethrin	13.2	9.67–18.4	13.3	10.6–16.8
Cypermethrin	>100		>100	
Bifenthrin	>100		>100	
PBO	1.03	0.751–1.39	1.09	0.751–1.53
1-ABT	176	123–254	215	118–491
Triflumizole	1.29	1.03–1.63	0.723	0.444–1.16
Prochloraz	0.235	0.182–0.302	0.059	0.0396–0.0861
Uniconazole	0.365	0.267–0.497	7.97	4.86–13.9
Propiconazole	6.95	4.27–11.3	2.38	1.72–3.28
Ketoconazole	3.71	2.74–5.06	0.518	0.396–0.675
Triadimefon	18	11.8–28.4	19.2	10.5–40.6
Triadimenol	>100		>100	
Tebuconazole	9.09	8.17–10.1	2.11	1.86–2.4
Epoxiconazole	21.4	15.3–36	44.7	20.1–159

of 235 nM and 59 nM for CYP6P9a and CYP6P9b, respectively (Table 1). The major differences were observed for ketoconazole, which showed ~7-fold stronger inhibition of CYP6P9b (IC_{50} 0.518 μM vs 3.71 μM), while uniconazole showed ~20-fold stronger inhibition of CYP6P9a (IC_{50} 0.365 μM vs 7.97 μM). All tested pyrethroids were weak inhibitors with IC_{50} values > 100 μM. In contrast, the pyrethroid metabolites 4′OH deltamethrin and 4′OH permethrin were relatively strong inhibitors with respective IC_{50} values of 6.28 μM and 13.2 μM for CYP6P9a and 1.75 μM and 13.4 μM for CYP6P9b. PBO also exhibited rather low IC_{50} values of approx. 1 μM against both CYP6P9a and CYP6P9b, whereas 1-ABT was ineffective at 100 μM (Table 1).

3.2. Metabolism of permethrin and deltamethrin by CYP6P9a and CYP6P9b

To investigate pyrethroid metabolism by CYP6P9a and CYP6P9b substrate turnover was measured following incubation with recombinantly expressed P450s (Figs. 2 and 3, Table S3). CYP6P9a produced similar levels of deltamethrin and permethrin depletion (~40%), whereas CYP6P9b produced slightly higher permethrin turnover (61.5%) compared with deltamethrin (40.4%) (Table S3). Compared with their respective parent compounds, both P450s produced significantly higher activity towards the 4′OH metabolites, with 65.3% and 67.3% depletion of 4′OH deltamethrin and 4′OH permethrin respectively for CYP6P9a and 68.9% and 74.3% depletion with CYP6P9b (Table S3).

Additional investigation of deltamethrin and permethrin metabolism by CYP6P9a and CYP6P9b by MS/MS revealed further metabolism of 4'OH deltamethrin and 4'OH permethrin to cyano-(3-hydroxyphenyl) methyl deltamethrate and 3-hydroxyphenyl-methyl-permethrate respectively via ether cleavage of the phenoxybenzyl moiety, which was confirmed by MS fragment spectra showing the respective M-76 metabolites and supported by molecular docking studies exemplified by CYP6P9b homology models (Fig. 4). Molecular docking of 4′OH metabolites into the active site of CYP6P9b revealed the aryl-ether of 4′OH permethrin coordinates closer to the heme iron centre than 4′OH deltamethrin with measured distances of 4.28 Å and 6.99 Å, respectively (Fig. 4A and B). Compared with deltamethrin, permethrin metabolism produced double the number of peaks in ESI-TOF UPLC-MS spectra (Fig. 4, Fig. S2). These are indicative of *cis*- and *trans*-permethrin isomers with different retention times, which was confirmed when matched against diastereomerically pure *cis*- and *trans*-permethrin with the same retention times.

Based on the analytical results there were no obvious differences in metabolism between deltamethrin and permethrin, except for an additional M+32 metabolite of permethrin produced by both P450s, suggesting a second hydroxylation site. Overall, the MS analysis supports the kinetics, which indicates very similar sequential oxidative substrate metabolism as outlined in Fig. 5. Interestingly, the ether bond cleavage in permethrin/4′OH permethrin was only detected for CYP6P9b, whereas the deltamethrin ether bond was cleaved by both enzymes (Fig. 5).

3.3. Acute toxicity of 4′OH pyrethroid metabolites against An. funestus

The acute contact efficacy of the metabolites 4′OH deltamethrin and 4′OH permethrin was tested against *An. funestus* strains FANG and FUMOZ-R to assess their intrinsic toxicity (Table 2). None of the metabolites was active against female adults of FUMOZ-R at the highest concentration, 100 mg/m^2, tested (Fig. S3). Interestingly, female adults of strain FANG showed an almost identical susceptibility to 4′OH deltamethrin (LC_{50}, 1.88 mg/m^2, CI95%: 0.72–3.89) and permethrin (LC_{50}, 0.543 mg/m^2, CI95%: 0.409–0.702 (Nolden et al., 2021)). Thus, suggesting that the detoxification of deltamethrin by hydroxylation only is not sufficient to render it ineffective in susceptible *An. funestus*, because intrinsically it remains almost as toxic as permethrin. Hydroxylated

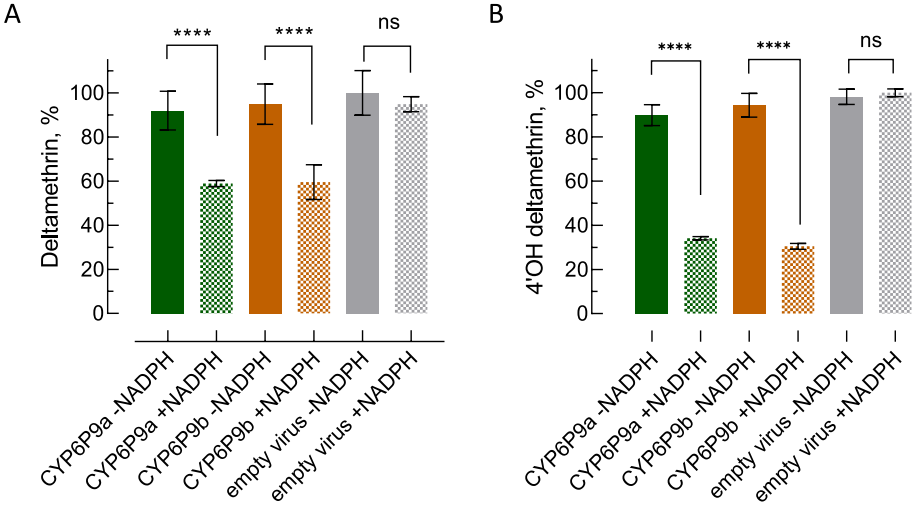

Fig. 2. Pyrethroid substrate metabolism by *An. funestus CYP6P9a and CYP6P9b.* Depletion of (A) deltamethrin and (B) 4′OH deltamethrin by recombinantly expressed CYP6P9a and CYP6P9b ± NADPH measured by quantitative UPLC-MS/MS. Remaining parent compound was determined after 90min incubation at 30 °C (starting concentration was 2 μM). Data were normalized to % parent compound and are mean values ± 95% CI (n = 3). Mock cells (empty virus) ± NADPH served as control. Original values are provided in Table S3.

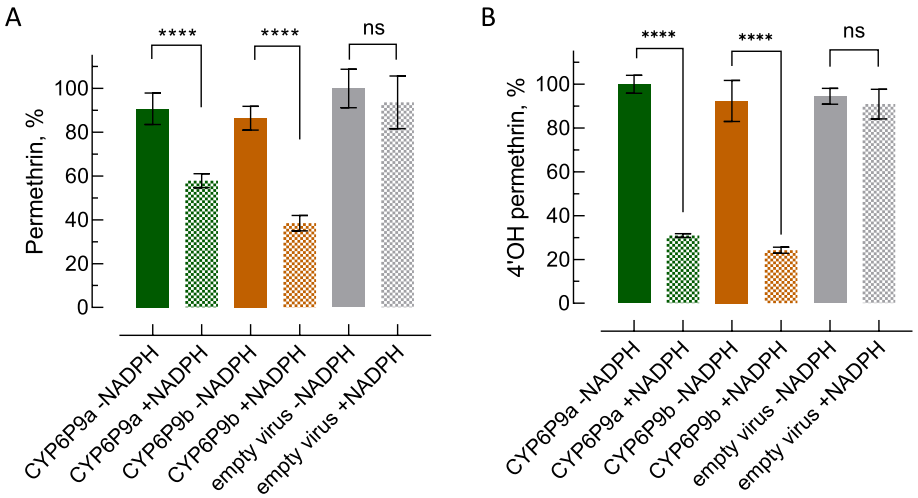

Fig. 3. Pyrethroid substrate metabolism by *An. funestus CYP6P9a and CYP6P9b.* Depletion of (A) permethrin and (B) 4′OH permethrin by recombinantly expressed CYP6P9a and CYP6P9b ± NADPH measured by quantitative UPLC-MS/MS. Remaining parent compound was determined after 90min incubation at 30 °C (starting concentration was 2.5 μM). Data were normalized to % parent compound and are mean values ± 95% CI (n = 3). Mock cells (empty virus) ± NADPH served as control. Original values are provided in Table S3.

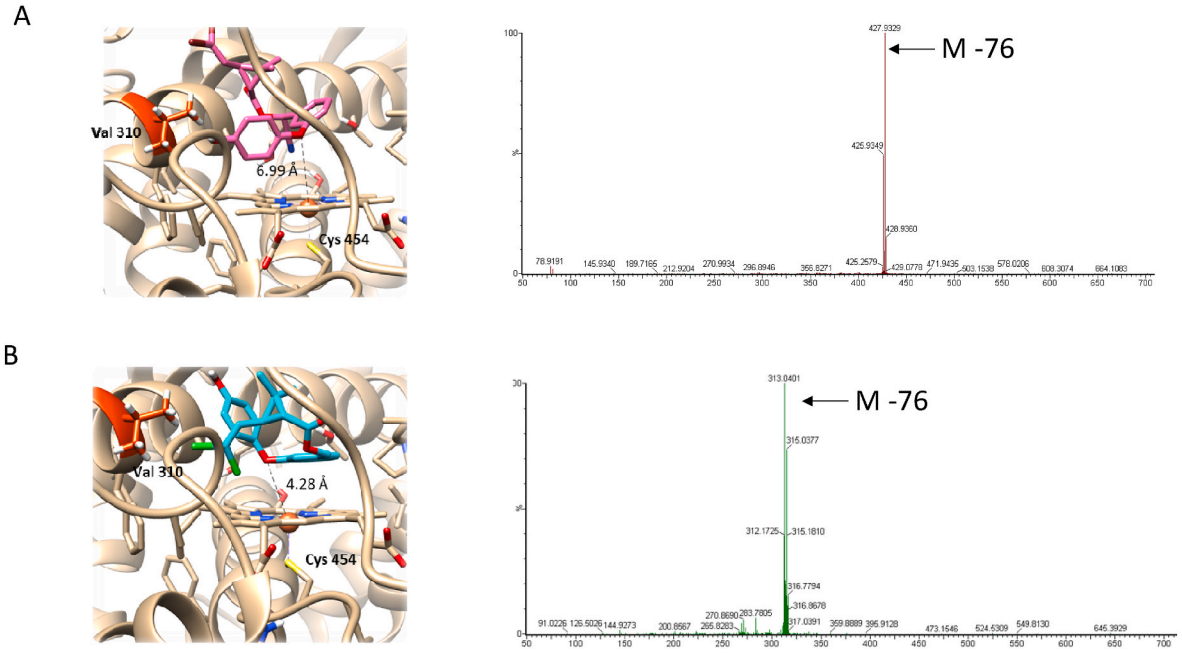

Fig. 4. Molecular docking and analytical validation. Binding site model showing the predicted substrate-binding mode of (A) 4′OH deltamethrin and (B) 4′OH permethrin in *An. funestus* CYP6P9b and the respective MS fragment spectra of the corresponding metabolites cyano-(3-hydroxyphenyl) methyl deltamethrate and 3-hydroxyphenyl-methyl-permethrate, respectively, as determined by ESI-TOF UPLC-MS.

permethrin showed an LC_{50} of 34.7 mg/m^2 and is approx. 20-fold less active than 4′OH deltamethrin (Table 2). In a previous study deltamethrin showed an LC_{50} of 4.61 mg/m^2 and 0.0206 mg/m^2 towards FUMOZ-R and FANG mosquitoes, respectively (Nolden et al., 2021).

3.4. Degradation and biological efficacy of permethrin diastereomers

Significantly different rates of hydroxylation of *cis*- and *trans*-permethrin diastereomers by CYP6P9a and CYP6P9b were observed by MS/MS analysis (Fig. 6A). Both enzymes preferentially depleted *trans*-permethrin over *cis*-permethrin, but CYP6P9b degraded *trans*-permethrin almost five-fold faster than CYP6P9a. To investigate toxicity differences towards susceptible FANG and pyrethroid resistant FUMOZ-R mosquitoes in relation to the low resistance ratio of permethrin (racemate) (RR 7.76; Nolden et al., 2021), diastereomerically pure *cis*- and *trans*-permethrin were evaluated in contact bioassays (Fig. 6B). The resistance ratios of *cis*- and *trans*-permethrin were 10.4 and 6.55, respectively (Table S4). However, *cis*-permethrin (LC_{50} 0.154 mg/m^2), had 9-times higher toxicity than *trans*-permethrin (LC_{50} 1.41 mg/m^2) towards FANG mosquitoes and 6 times higher toxicity to FUMOZ-R, LC_{50} 1.6 and 9.24 mg/m^2, respectively (Table S4).

3.5. Kinetics of CYP6P9 variants towards coumarin model substrates, type I and type II pyrethroids

The comparative metabolism of coumarin model substrates by CYP6P9a, CYP6P9b and their respective mutants CYP6P9a^{I310V} and CYP6P9b^{V310I} was investigated and generally followed Michaelis-Menten kinetics. Highest activity was measured with the benzylated coumarin BOMFC, with the four P450s producing similar rates of metabolism with V_{max} values in the range 167–196 pmol product/min x mg protein^{-1} (Fig. 7, Table S5). The K_m values for CYP6P9b and CYP6P9b^{V310I} were similar (6.82 and 7.16 μM, respectively) whereas the K_m value for CYP6P9a^{I310V} (3.21 μM) was 4-fold lower than CYP6P9a

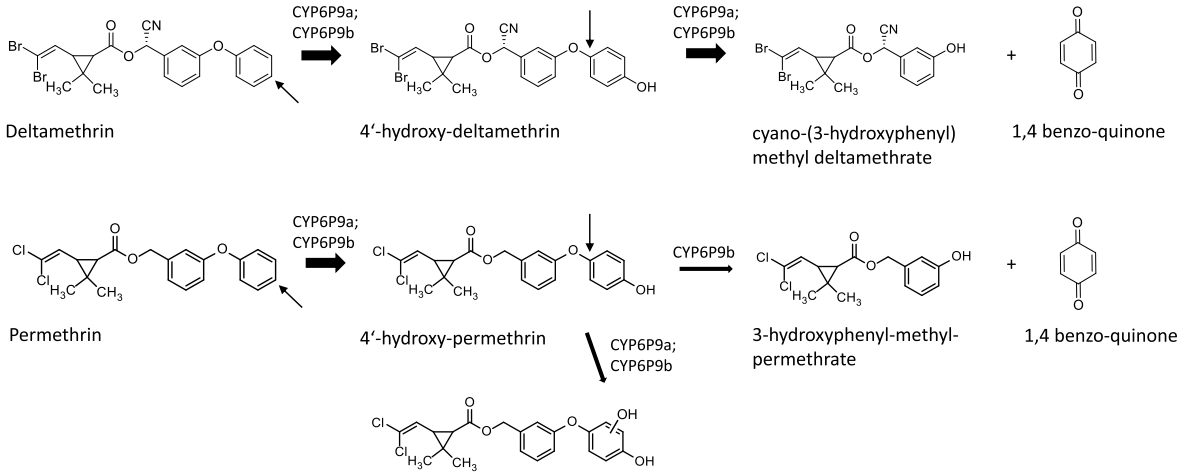

Fig. 5. Oxidative metabolic fate of pyrethroids. Proposed scheme for the sequential metabolism of deltamethrin and permethrin, respectively, mediated by recombinantly expressed *An. funestus* CYP6P9a and CYP6P9b supported by UPLC-MS analysis. Arrows indicate potential sites of oxidative attack.

Table 2
Efficacy of hydroxylated pyrethroids against *An. funestus*. Log-dose mortality data of 4′OH-deltamethrin and 4′OH permethrin against female adults of *An. funestus* FANG in glazed-tile contact bioassays. Both metabolites were inactive against female adults of strain FUMOZ-R at the highest concentration tested (100 mg/m^2). Respective graphs are given in the supporting information (Fig. S3).

	An. funestus FANG				
	LC_{50}	95% CI	Slope ± SE		n
4′OH deltamethrin	1.88	0.72–3.89	0.927	0.195	210
4′OH permethrin	34.7	15.8–91.7	0.953	0.242	210

(11.2 μM). The same trend was observed with BFC and EFC where CYP6P9a^{I310V} produced lower K_m values than the wildtype CYP6P9a with minimal change in V_{max} (Table S5). CYP6P9b and CYP6P9b^{V310I} produced similar V_{max} values with BFC (33.8 and 40.8 μM) and higher than CYP6P9a and CYP6P9a^{I310V} (11.0 and 8.78 μM). Most notably, CYP6P9b^{V310I} with a V_{max} of 55.3 pmol product/min x mg protein^{-1} was 4-5-fold more active against EFC than CYP6P9b and CYP6P9a and CYP6P9a^{I310V} (Fig. 7, Table S5).

Pyrethroid metabolism of the CYP6P9 variants was investigated by comparing the rates of production of the major 4′OH metabolites of deltamethrin and permethrin (Fig. 8). The highest reaction rate for deltamethrin was observed by CYP6P9b^{V310I} with a V_{max} of 13.7 pmol product/min x mg protein^{-1}, which was slightly higher than wildtype CYP6P9b (10.6 pmol product/min x mg protein^{-1}) but the same as CYP6P9a (Table S6). CYP6P9a^{I310V} produced the lowest deltamethrin activity of 6.65 pmol product/min x mg protein^{-1}. The amino acid substitution at position 310 produces a small reduction (~2-fold) in K_m values for CYP6P9a^{I310V} (7.6 μM) and CYP6P9b^{V310I} (14.7 μM) relative to CYP6P9a (19.2 μM) and CYP6P9b (27 μM) respectively (Table S6), indicating slightly higher affinity towards deltamethrin.

Compared with CYP6P9b (7.89 pmol product/min x mg protein^{-1}), CYP6P9a and CYP6P9a^{I310V} revealed relatively low activity towards permethrin with 1.97 and 3.07 pmol product/min x mg protein^{-1}, respectively (Table S6). Strikingly, the highest permethrin reaction rate was seen for CYP6P9b^{V310I} with 58 pmol product/min x mg protein^{-1}, a 7-fold increase compared with wildtype CYP6P9b (Fig. 8, Table S6). Metabolism of permethrin by CYP6P9^{V310I} also produced a sigmoidal curve and a linear Hanes-Woolf fit suggests an allosteric interaction and positive cooperativity, contrasting with the hyperbolic behaviour of the other P450s towards deltamethrin and permethrin (Fig. S4). Overall, the valine 310 to isoleucine substitution in CYP6P9b^{V310I} tended to enhance metabolic efficacy and produced higher affinity for all the inhibitors tested, whereas the reverse isoleucine to valine substitution at position 310 in CYP6P9a^{I310V} led to a weaker inhibition of all tested inhibitors (Table S7).

4. Discussion

Pyrethroid resistance in *An. funestus* is largely driven by the over-expression of duplicated P450s CYP6P9a and CYP6P9b, which have been shown to rapidly metabolise pyrethroids in functional assays employing prokaryotic and eukaryotic protein expression systems (Ibrahim et al., 2015; Nolden et al., 2022; Riveron et al., 2013; Yunta

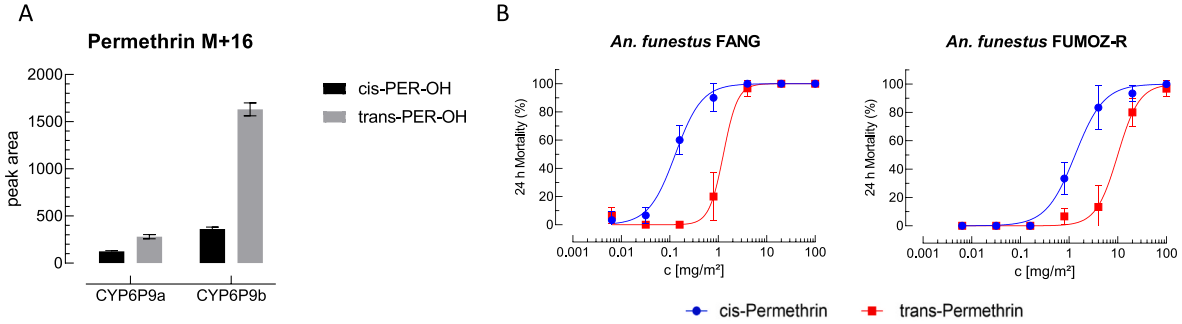

Fig. 6. Degradation and biological efficacy of permethrin enantiomers. (A) Resolution of enantioselective metabolism of permethrin to *cis/trans* 4′hydroxy permethrin by recombinantly expressed CYP6P9a and CYP6P9b in the presence of NADPH (90min). (B) Efficacy of *cis*- and *trans*-permethrin towards female adults of *An. funestus strains* FANG and FUMOZ-R in glazed tile contact assays. Data are mean values ± 95% CI (n = 3) and given in the supporting information (table S4).

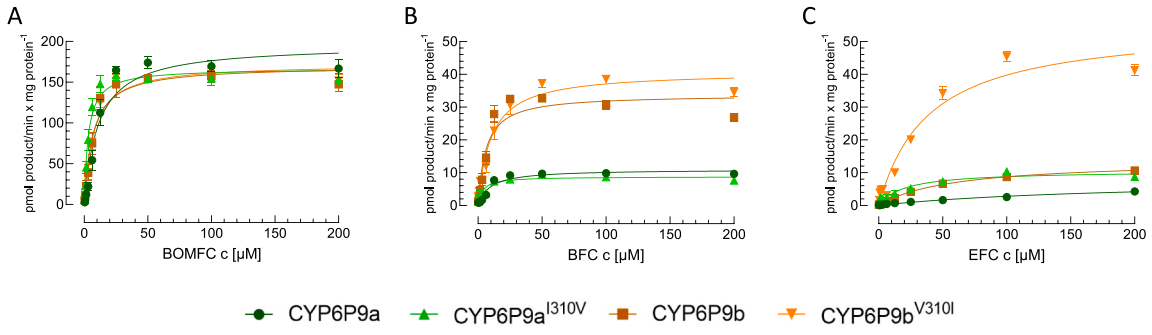

Fig. 7. Saturation kinetics of selected coumarin substrates with different *An. funestus* CYP6P9 variants. O-debenzylation of (A) 7-benzyloxymethoxy-4-trifluoromethylcoumarin (BOMFC) and (B) 7-benzyloxy-4-trifluoromethylcoumarin (BFC), as well as (C) the O-dealkylation of 7-ethoxy-4-trifluoromethylcoumarin (EFC) by recombinantly expressed CYP6P9a, CYP6P9b, CYP6P9aI310V and CYP6P9bV310I. Details on Michaelis-Menten kinetic data analysis are given in the supporting information (Table S5). Data are mean values ± SD (n = 4).

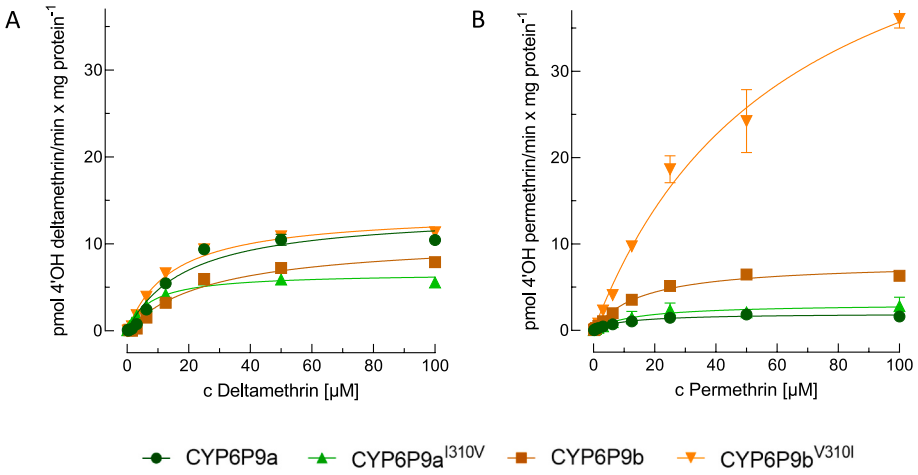

Fig. 8. Saturation kinetics of pyrethroid substrates with different *An. funestus* CYP6P9 variants. Hydroxylation of (A) deltamethrin and (B) permethrin by CYP6P9a, CYP6P9b, CYP6P9aI310V and CYP6P9bV310I. Details on Michaelis-Menten kinetic data analysis are given in the supporting information (Table S6). Data are mean values ± SD (n = 3).

et al., 2019). Previous studies mostly utilized parent depletion approaches (+NADPH vs -NADPH) to quantify the extent of pyrethroid metabolism by CYP6P9a and CYP6P9b (Ibrahim et al., 2016; Riveron et al., 2013, 2014), similar to P450 assays employed to predict pesticide clearance in mammalian toxicology (Scollon et al., 2009). We recently noticed a stochiometric inconsistency between deltamethrin depletion and 4′OH deltamethrin formation by functionally expressed CYP6P9 variants, and suggested the formation of additional, undetected metabolites (Nolden et al., 2022). Indeed, the present study revealed that the depletion of deltamethrin by recombinantly expressed CYP6P9a and CYP6P9b is principally based on sequential oxidative metabolism by, 1) hydroxylation of the 4′para position of the phenoxybenzyl ring, and 2) the formation of cyano-(3-hydroxyphenyl)-methyl-deltamethrate via ether cleavage of the phenoxybenzyl moiety. In addition, we confirmed sequential metabolism of the type I pyrethroid permethrin via the same route, but only for CYP6P9b. We failed to detect 3-hydroxyphenyl-methyl-permethrate in analytical assays with CYP6P9a, suggesting its lower catalytic capacity to oxidise 4′OH permethrin compared to CYP6P9b. This is supported by an overall higher permethrin depletion capacity of CYP6P9b compared to CYP6P9a, whereas no significant difference between both enzymes was detected for deltamethrin metabolism. Sequential P450-mediated metabolism of deltamethrin resulting in the formation of cyano-(3-hydroxyphenyl)-methyl-deltamethrate has so far only been described for *An. gambiae* CYP6M2 (Stevenson et al., 2011). Whereas CYP6P9b mediated ether cleavage of the phenoxybenzyl moiety of permethrin has been demonstrated for the first time in insects. A similar metabolic fate has so far only been observed in mammalian studies, e.g. with rat liver microsomes (Shono et al., 1979).

Interestingly, neither deltamethrin nor permethrin inhibited the *O*-debenzylation of BOMFC in a fluorescent probe assay we conducted with recombinantly expressed CYP6P9a and CYP6P9b, though we have detected low, but significant decrease of V_{max} values when both pyrethroids were tested at 100 µM. Indeed, the inhibitory efficacy of other pyrethroids such as bifenthrin and cypermethrin was also too low to calculate IC_{50}-values. Such fluorescence (and luminescence) probe assays have been successfully used to predict interaction and/or P450-mediated metabolism of insecticides, e.g., for *Bemisia tabaci* CYP6CM1 and imidacloprid (Hamada et al., 2019), *Apis mellifera* CYP9Q2/3 and various insecticides (Haas et al., 2021; Haas and Nauen, 2021), several mosquito P450s including *An. gambiae* CYP6P3 (Yunta et al., 2019), and *An. funestus* CYP6P9a/b for various insecticides including pyrethroids (Ibrahim et al., 2015, 2016; Yunta et al., 2019). Our results with BOMFC and pyrethroids are in contrast to diethoxyfluorescein probe assays with CYP6P9a/b where various insecticides have been shown to inhibit its *O*-dealkylation in the lower micromolar range, including deltamethrin and permethrin (Ibrahim et al., 2016; Yunta et al., 2019). However, a few insecticides tested by Yunta et al. (2019) such as DDT turned out to be micromolar inhibitors of CYP6P9a and other mosquito P450s but were not metabolised by recombinantly expressed enzymes. Our fluorescent probe assays with deltamethrin, and permethrin revealed the opposite, i.e., no significant inhibition of CYP6P9a/b, but substantial depletion in analytical assays. The azole compounds and PBO used to

validate the fluorescence probe assay have been described as strong *An. funestus* P450 inhibitors (Nolden et al., 2021), and showed strong inhibition of both CYP6P9a and CYP6P9b, not unexpected considering their *in vivo* potential as synergists in combination with pyrethroids (Horstmann and Sonneck, 2016; Williams et al., 2019). Further work is warranted to investigate the reasons for the discrepancy in pyrethroid inhibitory potential in fluorescent probe assays and metabolism.

Intriguingly, we observed a much stronger interaction in BOMFC fluorescent probe assays between CYP6P9a/b and the pyrethroid metabolites 4′OH-permethrin and 4′OH deltamethrin. The observed inhibition of the *O*-debenzylation of BOMFC by both hydroxy metabolites in fluorescent probe assays is linked to significantly higher CYP6P9a/b driven depletion rates in analytical assays when compared to the respective parent compound. To the best of our knowledge this is the first study investigating the oxidative metabolic fate of 4′para-hydroxylated pyrethroids by recombinantly expressed insect P450s. The MS fragment spectra of the resulting metabolites confirmed the formation of cyano-(3-hydroxyphenyl)-methyl deltamethrate and 3-hydroxyphenyl-methyl-permethrate and the sequential two-step reaction catalysed by either CYP6P9 variant. 4′OH-Deltamethrin is 100-fold less toxic than deltamethrin, but its intrinsic toxicity against *An. funestus* FANG remains high and is comparable to permethrin - thus clearly supporting the advantage of a two-step deltamethrin metabolisation mediated by upregulated CYP6P9 variants. Hydroxylated permethrin is much less toxic in bioassays and unlikely to confer phenotypic consequences by the lack of sequential metabolism mediated by CYP6P9a. A previous study suggested that high levels of pyrethroid-metabolising P450s in resistant *Brassicogethes aeneus* protect the pest by pyrethroid sequestration rather than facilitating 4′OH-deltamethrin formation, which has indeed been shown to be intrinsically moderately toxic to pollen beetles over-expressing CYP6BQ23 (Zimmer et al., 2014; Zimmer and Nauen, 2011).

Next, we investigated if the significant differences in permethrin depletion we observed between CYP6P9a and CYP6P9b are linked to stereoselectivity issues as permethrin is a diastereomeric mixture of *cis*- and *trans*-permethrin. Indeed, we detected a preference of both CYP6P9 variants to hydroxylate more readily *trans*-over *cis*-permethrin, with CYP6P9b exhibiting a significantly higher metabolic capacity and preference to hydroxylate *trans*-permethrin compared with CYP6P9a. As we did not analyse the metabolism of the hydroxylated isomers separately, we can only speculate – based on the metabolic fate of racemic 4′OH permethrin – that CYP6P9b is the main permethrin metaboliser, because it was shown to catalyse the ether cleavage of the phenoxybenzyl moiety at detectable levels, whereas CYP6P9a did not. Interestingly, mammalian P450s involved in permethrin metabolism seem to be consistently more active on *cis*-permethrin (Hedges et al., 2019), whereas the preferred route of *trans*-permethrin detoxification is hydrolytic via ester cleavage by esterases (Casida et al., 1983; Scollon et al., 2009; Shono et al., 1979). We then assessed the acute toxicity of both permethrin isomers and found that *cis*-permethrin was significantly more toxic than *trans*-permethrin against female adults of both *An. funestus* FANG and FUMOZ. Based on this result it is tempting to speculate that the metabolism of *cis*-permethrin might be reduced in the presence of its diastereomer *trans*-permethrin, i.e., *in vivo* retaining higher levels of the intrinsically more toxic *cis* isomer, possibly explaining the rather low levels of permethrin resistance (compared to deltamethrin) we recently described in our selected *An. funestus* FUMOZ-R laboratory strain (Nolden et al., 2021). It would be interesting to further investigate if racemic mixtures of pyrethroids are advantageous over enantiomerically pure compounds to control mosquitoes expressing P450-based metabolic resistance such as *An. funestus*.

Finally, we have carried out site-directed mutagenesis to create two mutants CYP6P9a^{I310V} and CYP6P9b^{V310I} to compare their metabolic activity with CYP6P9a and CYP6P9b towards permethrin, deltamethrin and coumarins. V310 is part of the catalytic site and the only residue in SRS4 of CYP6P9b different from CYP6P9a (I310). Furthermore, this site has been described mutated (V310I) in CYP6P9b haplotypes of a pyrethroid resistant field population of *An. funestus* from Benin (Ibrahim et al., 2015). Interestingly, we observed a striking increase in permethrin but not deltamethrin turnover by CYP6P9b^{V310I} compared with wildtype CYP6P9b, possibly explaining the high level of permethrin resistance observed in *An. funestus* strains from Benin showing this polymorphism. Ibrahim et al. (2015) described other key residues in CYP6P9b such as Val^{109}Ile, Asp^{335}Glu and Asn^{384}Ser as determinants of enhanced pyrethroid metabolism which has been confirmed by site-directed-mutagenesis as well. Here CYP6P9b^{V310I} showed a similar increase in the *O*-dealkylation of 7-EC, but not for the *O*-debenzylation of BFC and BOMFC. Whereas the swapped residue only weakly affected the catalytic capacity of the CYP6P9a variants towards coumarin substrates and pyrethroids. Indeed, mutations in substrate recognition sites of several insect P450s have been shown to be determinants of selectivity. For example in *An. gambiae* CYP6Z1 and CYP6Z2 differences in SRS1, SRS2 and SRS4 have been demonstrated to determine the capacity of CYP6Z1 to metabolise DDT (Chiu et al., 2008). In another study with different CYP6ER1-variants of *Nilaparvata lugens,* a hemipteran rice pest, a serine residue in SRS4 determined elevated imidacloprid metabolism (Zimmer et al., 2018). In the cotton bollworm, *Helicoverpa armigera,* variants of the CYP6AE subfamily with a valine to isoleucine substitution in SRS4 showed increased esfenvalerate metabolism (Shi et al., 2020). Similar observations were described for substitutions in SRS4 of human CYP2A1 and CYP2A2 leading to higher hydroxylation rates and alterations in ethoxy-coumarin *O*-dealkylation (Hanioka et al., 1992; Hiroya et al., 1994).

Nonetheless, further molecular work is warranted to shed light on the determinants of pyrethroid metabolism and resistance by CYP6P9 variants, and whether SRS4 residue 310 of CYP6P9b can potentially serve as a molecular marker of enhanced levels of pyrethroid resistance in *An. funestus*.

Declaration of competing interest

RN and MN are employed by Bayer AG (Germany), a manufacturer of pesticides. MN is also a PhD student affiliated with the Liverpool School of Tropical Medicine (UK), funded by the Innovative Vector Control Consortium (IVCC) and Bayer AG.

Acknowledgements

We greatly acknowledge the help of Johannes Glaubitz, Udo König and Birgit Nebelsiek with the UPLC-MS/MS analysis and Sebastian Horstmann and Uwe Pluschkell for their helpful discussion and comments.

Appendix A. Supplementary data

Supplementary data to this article can be found online at https://doi.org/10.1016/j.ibmb.2022.103813.

References

Abbott, W.S., 1925. A method of computing the effectiveness of an insecticide. J. Econ. Entomol. 18, 265–267. https://doi.org/10.1093/jee/18.2.265a.

Amenya, D.A., Naguran, R., Lo, T.-C.M., Ranson, H., Spillings, B.L., Wood, O.R., Brooke, B.D., Coetzee, M., Koekemoer, L.L., 2008. Over expression of a cytochrome P450 (CYP6P9) in a major african malaria vector. Insect Mol. Biol. 17, 19–25.

Bhatt, S., Weiss, D.J., Cameron, E., Bisanzio, D., Mappin, B., Dalrymple, U., Battle, K.E., Moyes, C.L., Henry, A., Eckhoff, P.A., Wenger, E.A., Briët, O., Penny, M.A., Smith, T. A., Bennett, A., Yukich, J., Eisele, T.P., Griffin, J.T., Fergus, C.A., Lynch, M., Lindgren, F., Cohen, J.M., Murray, C.L.J., Smith, D.L., Hay, S.I., Cibulskis, R.E., Gething, P.W., 2015. The effect of malaria control on Plasmodium falciparum in Africa between 2000 and 2015. Nature 526, 207–211. https://doi.org/10.1038/nature15535.

Brooke, B.D., Kloke, G., Hunt, R.H., Koekemoer, L.L., Tem, E.A., Taylor, M.E., Small, G., Hemingway, J., Coetzee, M., 2001. Bioassay and biochemical analyses of insecticide resistance in southern African Anopheles funestus (Diptera: Culicidae). Bull. Entomol. Res. 91, 265–272. https://doi.org/10.1079/ber2001108.

Casida, J.E., Gammon, D.W., Glickman, A.H., Lawrence, L.J., 1983. Mechanism of selective action of pyrethroid. Annu. Rev. Pharmacol. Toxicol. 413–438.
Chiu, T.L., Wen, Z., Rupasinghe, S.G., Schuler, M.A., 2008. Comparative molecular modeling of Anopheles gambiae CYP6Z1, a mosquito P450 capable of metabolizing DDT. Proc. Natl. Acad. Sci. U.S.A. 105, 8855–8860. https://doi.org/10.1073/pnas.0709249105.
Das, S., Garver, L., Dimopoulos, G., 2007. Protocol for mosquito rearing (A. gambiae). JoVE. https://doi.org/10.3791/221.
David, J., Ismail, H.M., Chandor-proust, A., Paine, M.J.I., 2013. Role of cytochrome P450s in insecticide resistance: impact on the control of mosquito-borne diseases and use of insecticides on Earth. Philos. Trans. R. Soc. B. https://doi.org/10.1098/rstb.2012.0429.
Feyereisen, R., 2019. Insect CYP Genes and P450 Enzymes, Reference Module in Life Sciences. https://doi.org/10.1016/b978-0-12-809633-8.04040-1.
Gleave, K., Lissenden, N., Richardson, M., Ranson, H., 2018. Piperonyl butoxide (PBO) combined with pyrethroids in long-lasting insecticidal nets (LLINs) to prevent malaria in Africa. Cochrane Database Syst. Rev. https://doi.org/10.1002/14651858.CD012776.
Gotoh, O., 1992. Substrate recognition sites in cytochrome P450 family 2 (CYP2) proteins inferred from comparative analyses of amino acid and coding nucleotide sequences. J. Biol. Chem. 267, 83–90. https://doi.org/10.1016/s0021-9258(18)48462-1.
Haas, J., Glaubitz, J., Koenig, U., Nauen, R., 2021. A mechanism-based approach unveils metabolic routes potentially mediating chlorantraniliprole synergism in honey bees, Apis mellifera L., by azole fungicides. Pest Manag. Sci. https://doi.org/10.1002/ps.6706.
Haas, J., Nauen, R., 2021. Pesticide risk assessment at the molecular level using honey bee cytochrome P450 enzymes : a complementary approach. Environ. Int. 147, 106372 https://doi.org/10.1016/j.envint.2020.106372.
Hamada, A., Wahl, G.D., Nesterov, A., Nakao, T., Kawashima, M., Banba, S., 2019. Differential metabolism of imidacloprid and dinotefuran by Bemisia tabaci CYP6CM1 variants. Pestic. Biochem. Physiol. 159, 27–33. https://doi.org/10.1016/j.pestbp.2019.05.011.
Hanioka, N., Gonzalez, F.J., Lindberg, N.A., Gao, L., Gelboin, H.V., Korzekwa, K.R., 1992. Site-directed mutagenesis of cytochrome P450s CYP2A1 and CYP2A2: influence of the distal helix on the kinetics of testosterone hydroxylation. Biochem. 31, 3364–3370. https://doi.org/10.1021/bi00128a009.
Hedges, L., Brown, S., MacLeod, A.K., Vardy, A., Doyle, E., Song, G., Moreau, M., Yoon, M., Osimitz, T.G., Lake, B.G., 2019. Metabolism of deltamethrin and cis- and trans-permethrin by human expressed cytochrome P450 and carboxylesterase enzymes. Xenobiotica 49, 521–527. https://doi.org/10.1080/00498254.2018.1474283.
Hiroya, K., Murakami, Y., Shimizu, T., Hatano, M., Ortiz De Montellano, P.R., 1994. Differential roles of Glu318 and Thr319 in cytochrome P450 1A2 catalysis supported by NADPH-cytochrome P450 reductase and tert-butyl hydroperoxide. Arch. Biochem. Biophys. https://doi.org/10.1006/abbi.1994.1184.
Horstmann, S., Sonneck, R., 2016. Contact bioassays with phenoxybenzyl and tetrafluorobenzyl pyrethroids against target-site and metabolic resistant mosquitoes. PLoS One 11, e0149738. https://doi.org/10.1371/journal.pone.0149738.
Ibrahim, S.S., Amvongo-Adjia, N., Wondji, M.J., Irving, H., Riveron, J.M., Wondji, C.S., 2018. Pyrethroid resistance in the major malaria vector anopheles funestus is exacerbated by overexpression and overactivity of the P450 CYP6AA1 across Africa. Genes 9, 1–17. https://doi.org/10.3390/genes9030140.
Ibrahim, S.S., Ndula, M., Riveron, J.M., Irving, H., Wondji, C.S., 2016. The P450 CYP6Z1 confers carbamate/pyrethroid cross-resistance in a major African malaria vector beside a novel carbamate-insensitive N485I acetylcholinesterase-1 mutation. Mol. Ecol. 25, 3436–3452. https://doi.org/10.1111/mec.13673.
Ibrahim, S.S., Riveron, J.M., Bibby, J., Irving, H., Yunta, C., Paine, M.J.I., Wondji, C.S., 2015. Allelic variation of cytochrome P450s drives resistance to bednet insecticides in a major malaria vector. PLoS Genet. 11, e1005618 https://doi.org/10.1371/journal.pgen.1005618.
Irving, H., Wondji, C.S., 2017. Investigating knockdown resistance (kdr) mechanism against pyrethroids/DDT in the malaria vector Anopheles funestus across Africa. BMC Genet. 18, 76. https://doi.org/10.1186/s12863-017-0539-x.
Martinez-Torres, D., Chandre, F., Williamson, M.S., Darriet, F., Berge, J.B., Devonshire, A.L., Guillet, P., Pasteur, N., Pauron, D., 1998. Molecular characterization of pyrethroid knockdown resistance (kdr) in the major malaria vector Anopheles gambiae s.s. Insect Mol. Biol. 7, 179–184.
Moyes, C.L., Lees, R.S., Yunta, C., Walker, K.J., Hemmings, K., Oladepo, F., Hancock, P. A., Weetman, D., Paine, M.J.I., Ismail, H.M., 2021. Assessing cross-resistance within the pyrethroids in terms of their interactions with key cytochrome P450 enzymes and resistance in vector populations. Parasites Vectors 14, 115. https://doi.org/10.1186/s13071-021-04609-5.
Nauen, R., Bass, C., Feyereisen, R., Vontas, J., 2022. The role of cytochrome P450s in insect toxicology and resistance. Annu. Rev. Entomol. 67, 105–124. https://doi.org/10.1146/annurev-ento-070621-061328.
Nolden, M., Brockmann, A., Ebbinghaus-kintscher, U., Brueggen, K., Horstmann, S., Paine, M.J.I., Nauen, R., 2021. Towards understanding transfl uthrin efficacy in a pyrethroid-resistant strain of the malaria vector Anopheles funestus with special reference to cytochrome P450-mediated detoxification. Curr. Res. Parasitol. Vector-Borne Dis. 1, 100041 https://doi.org/10.1016/j.crpvbd.2021.100041.
Nolden, M., Paine, M.J.I., Nauen, R., 2022. Biochemical profiling of functionally expressed CYP6P9 variants of the malaria vector Anopheles funestus with special reference to cytochrome b5 and its role in pyrethroid and coumarin substrate metabolism. Pestic. Biochem. Physiol. 182 https://doi.org/10.1016/j.pestbp.2022.105051.
Oleg, T., Olson, A.J., 2010. Software news and update AutoDock Vina: improving the speed and accuracy of docking with a new scoring function, efficient optimization, and multithreading. J. Comput. Chem. 31, 455–461. https://doi.org/10.1002/jcc.21334.
Omura, T., Sato, R., 1964. The carbon monoxide-binding pigment of liver microsomes. J. Biol. Chem. 239.
Paine, M.J.I., McLaughlin, L.A., Flanagan, J.U., Kemp, C.A., Sutcliffe, M.J., Roberts, G.C. K., Wolf, C.R., 2003. Residues glutamate 216 and aspartate 301 are key determinants of substrate specificity and product regioselectivity in cytochrome P450 2D6. J. Biol. Chem. 278, 4021–4027. https://doi.org/10.1074/jbc.M209519200.
Protopopoff, N., Mosha, J.F., Lukole, E., Charlwood, J.D., Wright, A., Mwalimu, C.D., Manjurano, A., Mosha, F.W., Kisinza, W., Kleinschmidt, I., Rowland, M., 2018. Effectiveness of a long-lasting piperonyl butoxide-treated insecticidal net and indoor residual spray interventions, separately and together, against malaria transmitted by pyrethroid-resistant mosquitoes: a cluster, randomised controlled, two-by-two fact. Lancet 391, 1577–1588. https://doi.org/10.1016/S0140-6736(18)30427-6.
Ranson, H., N'Guessan, R., Lines, J., Moiroux, N., Nkuni, Z., Corbel, V., 2011. Pyrethroid resistance in African anopheline mosquitoes: what are the implications for malaria control? Trends Parasitol. 27, 91–98. https://doi.org/10.1016/j.pt.2010.08.004.
Riveron, J.M., Ibrahim, S.S., Chanda, E., Mzilahowa, T., Cuamba, N., Irving, H., Barnes, K.G., Ndula, M., Wondji, C.S., 2014. The highly polymorphic CYP6M7 cytochrome P450 gene partners with the directionally selected CYP6P9a and CYP6P9b genes to expand the pyrethroid resistance front in the malaria vector Anopheles funestus in Africa. BMC Genom. 15, 817. https://doi.org/10.1186/1471-2164-15-817.
Riveron, J.M., Irving, H., Ndula, M., Barnes, K.G., Ibrahim, S.S., Paine, M.J.I., Wondji, C. S., 2013. Directionally selected cytochrome P450 alleles are driving the spread of pyrethroid resistance in the major malaria vector Anopheles funestus. Proc. Natl. Acad. Sci. USA 110, 252–257. https://doi.org/10.1073/pnas.1216705110.
Ruzo, L.O., Unai, T., Casida, J.E., 1978. Decamethrin metabolism in rats. J. Agric. Food Chem. 26, 918–925. https://doi.org/10.1021/jf60218a060.
Scollon, E.J., Starr, J.M., Godin, S.J., DeVito, M.J., Hughes, M.F., 2009. In vitro metabolism of pyrethroid pesticides by rat and human hepatic microsomes and cytochrome P450 isoforms. Drug Metab. Dispos. 37, 221–228. https://doi.org/10.1124/dmd.108.022343.
Shi, Y., O'Reilly, A.O., Sun, S., Qu, Q., Yang, Y., Wu, Y., 2020. Roles of the variable P450 substrate recognition sites SRS1 and SRS6 in esfenvalerate metabolism by CYP6AE subfamily enzymes in Helicoverpa armigera. Insect Biochem. Mol. Biol. 127, 103486 https://doi.org/10.1016/j.ibmb.2020.103486.
Shono, T., Ohsawa, K., Casida, J.E., 1979. Metabolism of trans-and cis-Permethrin, trans- and cis-Cypermethrin, and Decamethrin by Microsomal Enzymes. J. Agric. Food Chem. 27, 316–325. https://doi.org/10.1021/jf60222a059.
Soderlund, D.M., 2020. Neurotoxicology of pyrethroid insecticides. In: Neurotoxicity of Pesticides. Elsevier Inc., pp. 113–165. https://doi.org/10.1016/bs.ant.2019.11.002
Stevenson, B.J., Bibby, J., Pignatelli, P., Muangnoicharoen, S., O'Neill, P.M., Lian, L.Y., Müller, P., Nikou, D., Steven, A., Hemingway, J., Sutcliffe, M.J., Paine, M.J.I., 2011. Cytochrome P450 6M2 from the malaria vector Anopheles gambiae metabolizes pyrethroids: sequential metabolism of deltamethrin revealed. Insect Biochem. Mol. Biol. 41, 492–502. https://doi.org/10.1016/j.ibmb.2011.02.003.
WHO, 2021. World Malaria Report. World Malaria Report 2021.
WHO, 2020. World Malaria Report 2020. World Health Organization.
WHO, 2018. Global Report on Insecticide Resistance in Malaria Vectors: 2010-2016.
Williams, J., Flood, L., Praulins, G., Ingham, V.A., Morgan, J., Lees, R.S., Ranson, H., 2019. Characterisation of Anopheles strains used for laboratory screening of new vector control products. Parasites Vectors 12, 522. https://doi.org/10.1186/s13071-019-3774-3.
Wondji, C.S., Hearn, J., Irving, H., Wondji, M.J., Weedall, G., 2022. RNAseq-based gene expression profiling of the Anopheles funestus pyrethroid-resistant strain FUMOZ highlights the predominant role of the duplicated CYP6P9a/b cytochrome P450s. G3 Genes Genomes Genet. 12 https://doi.org/10.1093/G3JOURNAL/JKAB352.
Yunta, C., Hemmings, K., Stevenson, B., Koekemoer, L.L., Matambo, T., Pignatelli, P., Voice, M., Nász, S., Paine, M.J.I., 2019. Cross-resistance profiles of malaria mosquito P450s associated with pyrethroid resistance against WHO insecticides. Pestic. Biochem. Physiol. 161, 61–67. https://doi.org/10.1016/j.pestbp.2019.06.007.
Zimmer, C.T., Bass, C., Williamson, M.S., Kaussmann, M., Wölfel, K., Gutbrod, O., Nauen, R., 2014. Molecular and functional characterization of CYP6BQ23, a cytochrome P450 conferring resistance to pyrethroids in European populations of pollen beetle, Meligethes aeneus. Insect Biochem. Mol. Biol. 45, 18–29. https://doi.org/10.1016/j.ibmb.2013.11.008.
Zimmer, C.T., Garrood, W.T., Singh, K.S., Randall, E., Lueke, B., Gutbrod, O., Matthiesen, S., Kohler, M., Nauen, R., Davies, T.G.E., Bass, C., 2018. Neofunctionalization of duplicated P450 genes drives the evolution of insecticide resistance in the Brown planthopper. Curr. Biol. 28, 268–274. https://doi.org/10.1016/j.cub.2017.11.060 e5.
Zimmer, C.T., Nauen, R., 2011. Cytochrome P450 mediated pyrethroid resistance in European populations of Meligethes aeneus (Coleoptera: nitidulidae). Pestic. Biochem. Physiol. 100, 264–272. https://doi.org/10.1016/j.pestbp.2011.04.011.